2021 43rd Annual International Conference of the
IEEE Engineering in Medicine & Biology Society (EMBC)
Oct 31 - Nov 4, 2021. Virtual Conference

Cruciate-Ligament-Inspired Compliant Joints: Application to 3D-Printed Continuum Surgical Robots

Yilun Sun, *Graduate Student Member, IEEE*, and Tim C. Lueth, *Senior Member, IEEE*

***Abstract*— The rapid development of additive manufacturing technology makes it possible to fabricate a patient-specific surgical robot in a short time. To simplify the assembly process of the printed robotic system, compliant-joint-based monolithic structures are often used as substitutes for rigid-link mechanisms to realize flexible bending. In this paper, we introduce a cruciate-ligament-inspired compliant joint (CLCJ) to improve the bending stability of the 3D-printed continuum surgical robots. The basic structure of the tendon-driven CLCJ mechanism and its kinematic model were described in detail. The bending performance of CLCJ was also successfully evaluated by FEM simulation and experimental tests. Besides, a prototype of CLCJ-based surgical robotic system was presented to demonstrate its application in 3D-printed continuum surgical robots.**

I. Introduction

In recent years, research on patient-specific medical robots has attracted much attention. The increased demand for patient-specific robots is due to the fact that surgical intervention approaches and operation workspaces can vary greatly for patients of different ages and genders [1]. In order to achieve just-in-time manufacturing of patient-specific robots with complex shapes, the 3D printing technology is frequently used because of its high efficiency and high design freedom. According to their kinematics, the 3D-printed surgical robots can be divided into two categories: rigid-link-based robots and continuum robots. For the first category, a typical example was presented in [2], where a 3D-printed reconfigurable surgical robot was developed for endoluminal surgery, using printed revolute joints and gears for motion transmissions. The main limitation of the rigid-link-based surgical robots is that, a lot of laborious work is still required to assemble the separately printed components. To cope with this problem, continuum structure based mechanisms, as in the second category, are incorporated into the design of 3D-printed surgical robots, whose motion is based on elastic deformation of the flexible members in the structure. For instance, an elastic concentric tube robot was developed by Morimoto and Okamura using the selective laser sintering (SLS) technology [3]. The same 3D-printing technology was also utilized in our institute to fabricate tendon-driven continuum robots for patient-specific applications [4], [5].

In our previous studies [4], [5], notch-hinge-based compliant joints (NHCJ) were successfully used to achieve flexible bending of the tendon-driven continuum robots. However, the mechanical stress in a largely deflected NHCJ is unevenly distributed, which could lead to fatigue or even fracture of the continuum robotic structure [6]. To cope with this problem, we present a cruciate-ligament-inspired compliant joint (CLCJ) in this paper to improve the mechanical performance of the 3D-printed continuum robots (see Fig. 1a). Herein, the concept of cruciate ligaments was incorporated into our design because the anterior and posterior cruciate ligament act like two cross-axis ropes that can effectively protect the human knees and make the rotating movements between the femur and tibia stable (see Fig. 1b).

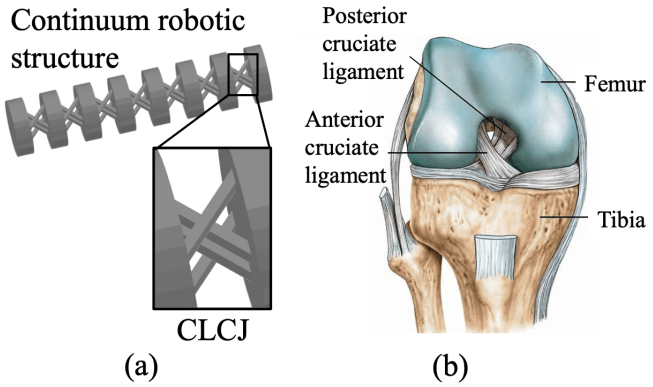

Fig. 1. Comparison of the CLCJ structure and the cruciate ligaments in human knees: a) A continuum robotic structure based on CLCJs, b) The anatomy of cruciate ligaments in the knee.

The remainder of the paper is organized as follows: Section II describes the basic geometry of the CLCJ-based continuum structure and the tendon-driven actuation mechanism. A kinematic model is also provided. In Section III, results of FEM-based simulation and experimental tests are presented to verify the bending performance and the kinematic model of the continuum structure. Section IV presents an SLS-printed CLCJ-based surgical robot to demonstrate the application of the bionic joints in medical robots. The entire work is concluded in Section V. Future work is also outlined.

II. Design of CLCJ-Based Continuum Structure

A. Structure of a Single CLCJ

As is shown in Fig. 1a), a CLCJ-based continuum structure is comprised of a set of repetitive rigid circular disks and flexible CLCJs. In our design, the goal of a single CLCJ (see Fig. 2) is to achieve 1-degree-of-freedom (1-DOF) rotation along the z-axis. Since the original cross-axis two-beam

This work was supported by the Munich School of Robotics and Machine Intelligence (MSRM), Technical University of Munich, Munich, Germany.

The authors are with the Institute of Micro Technology and Medical Device Technology, Technical University of Munich, Munich, Germany (e-mail: yilun.sun@tum.de; tim.lueth@tum.de).

Corresponding author: Yilun Sun.

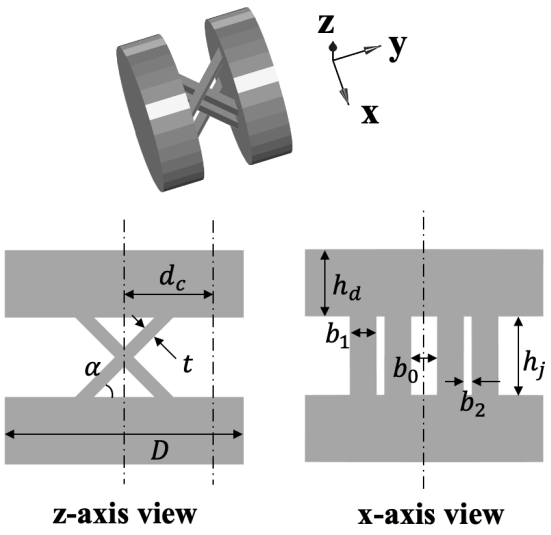

Fig. 2. Structure of a single CLCJ (marked with parameters).

TABLE I
VALUES OF THE DESIGN PARAMETERS FOR CLCJ

Parameter	Symbol	Value
Diameter of the rigid circular disk	D	9 mm
Distance between two neighboring disks	h_j	3 mm
Thickness of a disk	h_d	2.5 mm
Thickness of a single beam	t	0.5 mm
Inclination angle of a beam	α	45°
Gap for central cable routing	b_0	1 mm
Width of a beam	b_1	1 mm
Gap between two cross-axis beams	b_2	0.3 mm
Distance between central line and side cable	d_c	3.5 mm

structure (anterior and posterior cruciate ligament) may cause unwanted out-of-plane displacements when actuated by in-plane moments [7], we have incorporated four symmetrical cross-axis beams into the CLCJ to improve its in-plane bending performance (see Fig. 2). The values of several important parameters are listed in Table I. It should be mentioned that, the small gap b_2 between the neighboring cross-axis beams was constructed to avoid merging of the beams during the SLS printing process. The inclination angle α was chosen as $45°$ according to the previous study on cross-axis pivots [8], while the beam thickness t was set to $0.5\,\mathrm{mm}$ based on our preliminary study on SLS-printable flexure hinges [6].

Using the analytical methods in [9], the rotational stiffness of a CLCJ in x, y and z axis can be calculated as:

$$K_{\theta_x} = \frac{M_x}{\theta_x} = \frac{14Eb_1^3 t \sin\alpha}{3h_j} + \frac{Eb_1 t^3 \sin\alpha}{3h_j(\nu+1)} \tag{1}$$

$$K_{\theta_y} = \frac{M_y}{\theta_y} = \frac{2Eb_1^3 t \sin\alpha}{3h_j} + \frac{4Eb_1^3 t^3 (\sin\alpha)^3}{h_j^3} + \frac{Eb_1 t^3 \sin\alpha}{3h_j(\nu+1)} \tag{2}$$

$$K_{\theta_z} = \frac{M_z}{\theta_z} = \frac{Eb_1 t^3 \sin\alpha}{3h_j} \tag{3}$$

where K_{θ_x}, K_{θ_y} and K_{θ_z} are the obtained rotational stiffnesses. $E = 1700$MPa and $\nu = 0.3$ are the elastic modulus and Poisson's ratio of the printing material PA2200 (EOS GmbH, Germany). θ_x, θ_y and θ_z are the decoupled rotational angles induced by the in-plane moments M_x, M_y and M_z, respectively. From (1), (2) and (3), the stiffness ratios of $K_{\theta_x}/K_{\theta_z}$ and $K_{\theta_y}/K_{\theta_z}$ can be calculated as:

$$\frac{K_{\theta_x}}{K_{\theta_z}} = \frac{14b_1^2}{t^2} + \frac{1}{\nu+1} \approx 56.8 \gg 1 \tag{4}$$

$$\frac{K_{\theta_y}}{K_{\theta_z}} = \frac{2b_1^2}{t^2} + \frac{12b_1^2(\sin\alpha)^2}{h_j^2} + \frac{1}{\nu+1} \approx 9.4 \gg 1 \tag{5}$$

Since both $K_{\theta_x}/K_{\theta_z}$ and $K_{\theta_y}/K_{\theta_z}$ are much greater than 1, we can see that the CLCJ can effectively resist the torsional moments along the x and y axis. From this point of view, the bionic joint is able to perform stable in-plane rotation along the z axis.

B. Tendon-Driven Actuation Mechanism

The bending movements of the CLCJ-based continuum structure were actuated by a tendon-driven mechanism. To reduce the transmission backlash, we developed a Bowden-cable-integrated linear actuation system, as is shown in Fig. 3a). Since the Bowden cable can transmit both pull and push forces, we used a single cable to realize the back and forth bending of a single segment of the continuum structure, in which the CLCJs have the identical rotation orientation. In addition, a compliant slider mechanism (see Fig. 3b) was also developed to actuate the Bowden cable, whose displacement could be controlled manually or by computer algorithms.

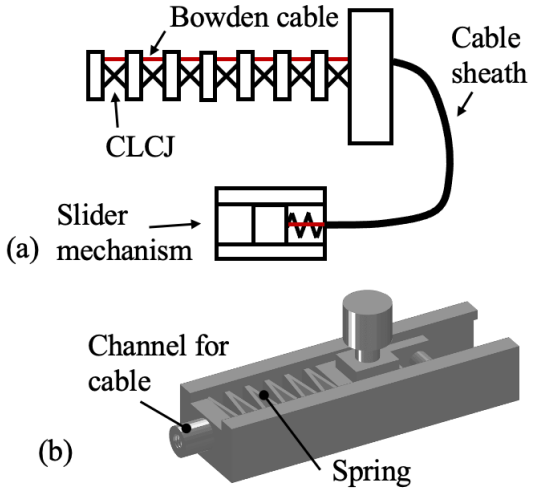

Fig. 3. Bowden-cable-integrated linear actuation system: a) Schematic diagram of the tendon-driven actuation mechanism, b) A compliant slider mechanism to control the cable.

C. Kinematic Modeling

In this section, we used the constant curvature method (CCM) [10] to describe the kinematics of the CLCJ-based continuum robotic structure. Herein, a single segment of the continuum robot was taken into account, which consists of n basic CLCJs. A schematic diagram was presented in Fig. 4 to describe the CCM-based kinematic model, whose deflection

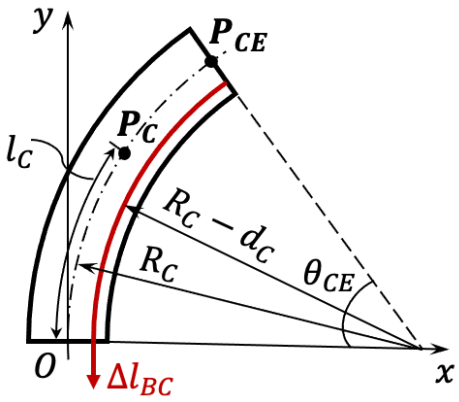

Fig. 4. A schematic diagram of the kinematic model for the CLCJ-based continuum robotic structure.

occurs in the x-y plane. According the CCM theory, the center line of the continuum robot is considered as a circular arc with a radius of R_C and a constant arc length of l_{CE}. $\boldsymbol{P}_{CE}$ and θ_{CE} are the end point and the angle of the arc, respectively. $\boldsymbol{P}_C$ depicts an arbitrary point on the central arc. The cable actuation length is denoted by Δl_{BC}.

The kinematic constraints due to the constant arc length can be formulated as:

$$l_{CE} = R_C\theta_{CE} = n(h_j + h_d) \tag{6}$$

$$\Delta l_{BC} = R_C\theta_{CE} - (R_C - d_c)\theta_{CE} = d_c\theta_{CE} \tag{7}$$

Let Δl_{BC} be the variable, R_C and θ_{CE} can be calculated from (6) and (7) as:

$$R_C = \frac{nd_c(h_j + h_d)}{\Delta l_{BC}} \tag{8}$$

$$\theta_{CE} = \frac{\Delta l_{BC}}{d_c} \tag{9}$$

On the other hand, the coordinates of $\boldsymbol{P}_{CE}$ and $\boldsymbol{P}_C$ can be described as:

$$\begin{cases} x_{CE} = R_C(1 - \cos\theta_{CE}) \\ y_{CE} = R_C \sin\theta_{CE} \end{cases} \tag{10}$$

$$\begin{cases} x_C = R_C(1 - \cos(\frac{l_C}{R_C})) \\ y_C = R_C \sin(\frac{l_C}{R_C}) \end{cases} \tag{11}$$

Substituting (8) and (9) into (10) and (11) yields:

$$\begin{cases} x_{CE}(\Delta l_{BC}) = \frac{nd_c(h_j + h_d)}{\Delta l_{BC}}(1 - \cos(\frac{\Delta l_{BC}}{d_c})) \\ y_{CE}(\Delta l_{BC}) = \frac{nd_c(h_j + h_d)}{\Delta l_{BC}} \sin(\frac{\Delta l_{BC}}{d_c}) \end{cases} \tag{12}$$

$$\begin{cases} x_C(\Delta l_{BC}, l_C) = \frac{nd_c(h_j + h_d)}{\Delta l_{BC}}(1 - \cos(\frac{l_C\Delta l_{BC}}{nd_c(h_j + h_d)})) \\ y_C(\Delta l_{BC}, l_C) = \frac{nd_c(h_j + h_d)}{\Delta l_{BC}} \sin(\frac{l_C\Delta l_{BC}}{nd_c(h_j + h_d)}) \end{cases} \tag{13}$$

which present the forward kinematics of the cable-driven CLCJ-based continuum robotic structure.

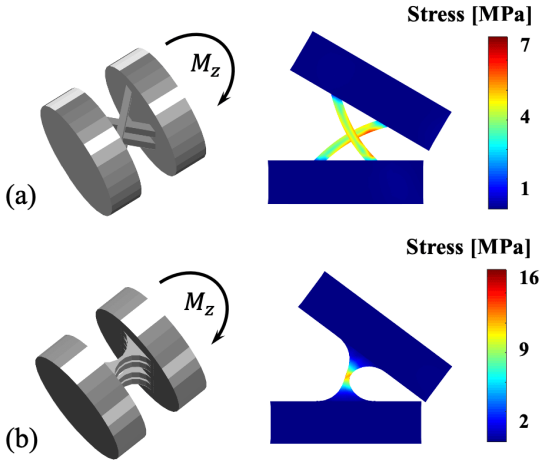

Fig. 5. Comparison of the stress distribution of a CLCJ and an NHCJ under the z-axis moment M_z: a) The stresses inside the CLCJ were evenly distributed along the cross-axis beams, b) The stresses inside the NHCJ were highly concentrated in the notch hinges.

III. Evaluation of the Bending Performance

A. FEM-Based Stress Analysis

In this section, large-displacement FE-simulation [11] was performed to analyze the stresses in a CLCJ under the z-axis moment (see Fig. 5a). The stresses in an NHCJ for the same loading condition were also analyzed for comparison (see Fig. 5b). From the simulation results, it can be noticed that the stress distribution of CLCJ is more even than that of NHCJ, which shows the better mechanical performance of CLCJ.

B. In-Plane Bending Tests

To validate the kinematic model described in Section II-C, in-plane bending tests were conducted. The experimental setup is presented in Fig. 6, where a continuum robotic structure made of 7 CLCJs was used for bending. A digital microscope (Conrad DP-M17) was used to measure the coordinates of the center-line point $\{\boldsymbol{P}_i\}_{i=1,2,\ldots,7}$ on each disk during the bending movement. In the experiment, the continuum structure was actuated by the Bowden cable to reach 4 poses with Δl_{BC} of $-\pi d_c/2$, $-\pi d_c/4$, $\pi d_c/4$ and $\pi d_c/2$. Fig. 7a) shows the deflected shape in the 1st and 4th pose. The measured results are reported in the blue curves in Fig. 7b), where each measurement was repeated for 3 times

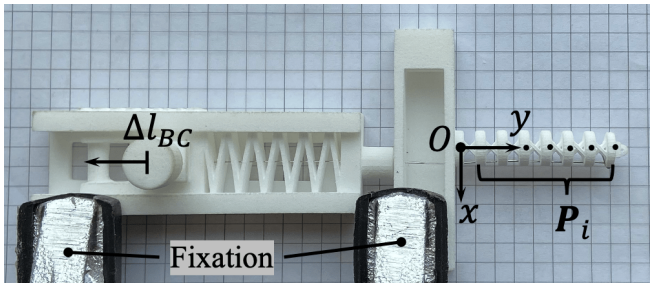

Fig. 6. Experimental setup for the in-plane bending tests.

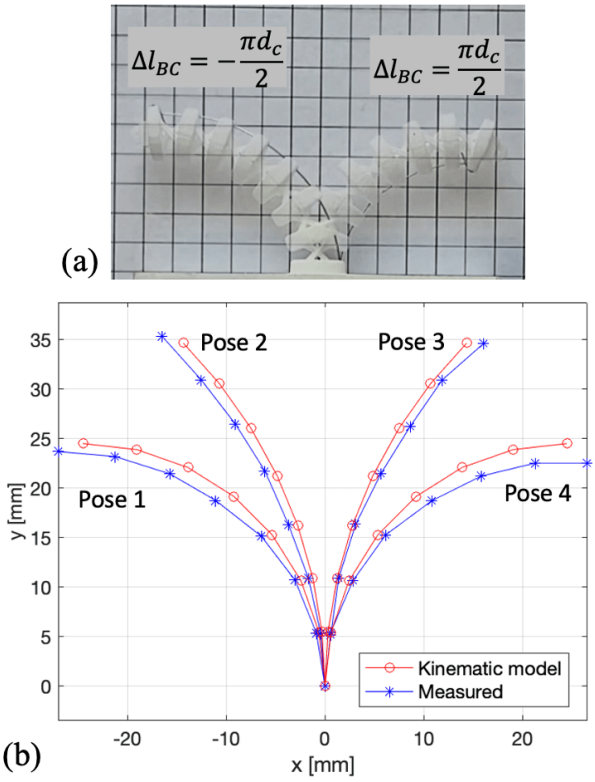

Fig. 7. Experimental results: a) The deflected shapes of the continuum structure with Δl_{BC} of $-\pi d_c/2$ and $\pi d_c/2$, b) A comparison of the calculated (red) and measured (blue) coordinates of $\boldsymbol{P}_i$ in the 4 poses. Δl_{BC} are $-\pi d_c/2$, $-\pi d_c/4$, $\pi d_c/4$ and $\pi d_c/2$ in the 4 poses.

to improve the credibility of the results. Compared to the analytical results (the red curves) calculated by the kinematic model in (13), the maximum coordinate difference is only 2.0 mm, which means the in-plane bending movements of the CLCJ-based continuum structure can be well described by the CCM-based kinematic model.

IV. Application to 3D-Printed Surgical Robot

To demonstrate the the application of CLCJ, an SLS-printed continuum surgical robot was presented in Fig. 8, in which two segments of the CLCJ-based continuum structures (from Section III-B) are incorporated. The orientation of the CLCJs in segment 1 was vertical to that of segment 2 so that the continuum robot can realize 2-DOF bending.

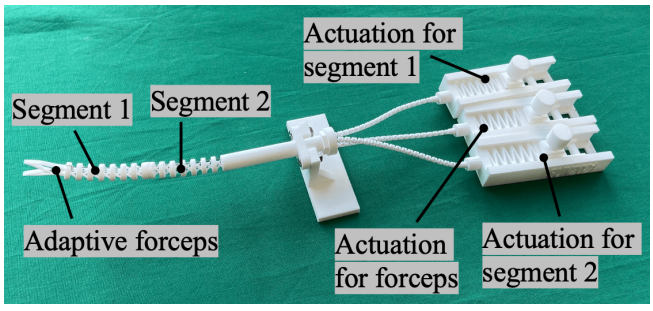

Fig. 8. A CLCJ-based 3D-printed continuum surgical robot.

A topology-optimized forceps [12] was also attached to the tip of the robot to perform adaptive grasping of sensitive tissues. Besides, the flexible-bending segments and the forceps were all actuated by the tendon-driven mechanisms described in Section II-B. Since the 3D-printed components are all parametrically designed by our modeling toolbox in MATLAB [13], the size of the presented continuum robot can be easily adapted to patient-specific requirements.

V. Conclusion and Future Work

In this paper, we presented a cruciate-ligament-inspired compliant joint (CLCJ) to improve the bending stability of 3D-printed continuum surgical robots. The mechanical performance and kinematics of the CLCJ-based continuum structure were successfully evaluated by FE-simulation and experimental tests. In future work, multidimensional payload tests should be carried out to evaluate the loading capacity of CLCJ. Besides, we will analyze the effect of different sizes on the performance of CLCJ to explore its potential for manufacturing patient-specific surgical robots.

References

[1] J. P. Desai, J. Sheng, S. S. Cheng, X. Wang, N. J. Deaton, and N. Rahman, "Toward patient-specific 3d-printed robotic systems for surgical interventions," *IEEE Transactions on Medical Robotics and Bionics*, vol. 1, no. 2, pp. 77–87, 2019.

[2] K. Harada, E. Susilo, A. Menciassi, and P. Dario, "Wireless reconfigurable modules for robotic endoluminal surgery," in *2009 IEEE International Conference on Robotics and Automation*, pp. 2699–2704, 2009.

[3] T. K. Morimoto and A. M. Okamura, "Design of 3-d printed concentric tube robots," *IEEE Transactions on Robotics*, vol. 32, no. 6, pp. 1419–1430, 2016.

[4] Y. S. Krieger, D. B. Roppenecker, I. Kuru, and T. C. Lueth, "Multi-arm snake-like robot," in *2017 IEEE International Conference on Robotics and Automation (ICRA)*, pp. 2490–2495, 2017.

[5] S. V. Brecht, M. Stock, J. Stolzenburg, and T. C. Lueth, "3d printed single incision laparoscopic manipulator system adapted to the required forces in laparoscopic surgery," in *2019 IEEE/RSJ International Conference on Intelligent Robots and Systems (IROS)*, pp. 6296–6301, 2019.

[6] Y. S. Krieger, C. M. Kuball, D. Rumschoettel, C. Dietz, J. H. Pfeiffer, D. B. Roppenecker, and T. C. Lueth, "Fatigue strength of laser sintered flexure hinge structures for soft robotic applications," in *2017 IEEE/RSJ International Conference on Intelligent Robots and Systems (IROS)*, pp. 1230–1235, 2017.

[7] Z. Hongzhe and B. Shusheng, "Accuracy characteristics of the generalized cross-spring pivot," *Mechanism and Machine Theory*, vol. 45, no. 10, pp. 1434–1448, 2010.

[8] B. D. Jensen and L. L. Howell, "The modeling of cross-axis flexural pivots," *Mechanism and Machine Theory*, vol. 37, no. 5, pp. 461–476, 2002.

[9] Y. Bellouard, *Microrobotics: Methods and Applications*. CRC Press, 1 ed., 2009.

[10] I. Robert J. Webster and B. A. Jones, "Design and kinematic modeling of constant curvature continuum robots: A review," *The International Journal of Robotics Research*, vol. 29, no. 13, pp. 1661–1683, 2010.

[11] Y. Sun, D. Zhang, Y. Liu, and T. C. Lueth, "Fem-based mechanics modeling of bio-inspired compliant mechanisms for medical applications," *IEEE Transactions on Medical Robotics and Bionics*, vol. 2, no. 3, pp. 364–373, 2020.

[12] Y. Sun, Y. Liu, L. Xu, Y. Zou, A. Faragasso, and T. C. Lueth, "Automatic design of compliant surgical forceps with adaptive grasping functions," *IEEE Robotics and Automation Letters*, vol. 5, no. 2, pp. 1095–1102, 2020.

[13] Y. Sun and T. C. Lueth, "Sgcl: A b-rep-based geometry modeling language in matlab for designing 3d-printable medical robots," in *2021 IEEE International Conference on Automation Science and Engineering (CASE)*, 2021.